Geophys. J. Int. (2009) **179,** 1039–1054 doi: 10.1111/j.1365-246X.2009.04313.x

High resolution Q^{-1} estimation based on extension of coda normalization method and its application to *P*-wave attenuation structure in the aftershock area of the 2005 West Off Fukuoka Prefecture Earthquake (*M*7.0)

S. Matsumoto,[1] K. Uehira,[1] A. Watanabe,[4] K. Goto,[2] Y. Iio,[3] N. Hirata,[4] T. Okada,[5] H. Takahashi,[6] H. Shimizu,[1] M. Shinohara[4] and T. Kanazawa[4]

[1]*Institute of Seismology and Volcanology, Kyushu University, Japan. E-mail: matumoto@sevo.kyushu-u.ac.jp*
[2]*Faculty of Sciences, Kagoshima University, Japan*
[3]*Disaster Prevention Research Institute, Kyoto University, Japan*
[4]*Earthquake Research Institute, University of Tokyo, Japan*
[5]*Graduate School of Science, Tohoku University, Japan*
[6]*Graduate School of Science, Hokkaido University, Japan*

Accepted 2009 June 25. Received 2009 June 24; in original form 2008 September 25

SUMMARY

We developed a method for estimating the seismic-wave attenuation ($1/Q$) in a seismically active region such as an aftershock area. To estimate the attenuation factor between two adjacent hypocentres, we employed two seismograms recorded at a station and calculate the ratio between two power spectra of direct waves normalized by those in the coda for both the events. The coda normalization of the spectrum and the ratio between the two events minimize the possible influences of sources, sites, instruments and attenuation from the station to the hypocentral area. The $1/Q$ value can be estimated from the variation of the ratios of event pairs calculated at many stations for various traveltime differences between the even pairs. This method involves double-difference (DD) estimation from the logarithmic power spectra for estimating the $1/Q$ structure, employing a concept similar to the recently developed 'DD tomography' for velocity structures. We applied this method to the aftershock area of the 2005 West Off Fukuoka Prefecture Earthquake (M7.0) in order to investigate the $1/Q$ structure of P waves. By using the spectra of the seismograms of 1781 events recorded at a dense seismic network deployed around the aftershock area, we obtained the spatial variation of the $1/Q$ value in this region. The $1/Q$ distribution thereby obtained suggests that there exists a high-attenuation region around the edge of the main shock fault, which could correspond to the segment boundary between the earthquake fault and the adjacent faults. In addition, we found that the initiation points of the main shock and aftershocks were located in a low-attenuation region.

Keywords: Body waves; Seismic attenuation; Seismic tomography; Wave scattering and diffraction.

INTRODUCTION

The seismic attenuation ($1/Q$) value is a measure of the property of a medium in attenuating seismic wave energy, $1/Q$ which provides us with important physical information about the Earth's interior. As reviewed by Sato & Fehler (1998), there are two factors causing this attenuation: (1) intrinsic absorption due to which the kinetic energy of seismic waves is converted into thermal energy by either internal friction on the cracks existing in the medium or by viscoelastic deformation and (2) the energy loss from the propagating seismic wave front caused by the scattering phenomenon due to the heterogeneity of the medium.

The spatial distribution of $1/Q$ is indicative of either the temperature and anelastic behaviours of the medium or the fluctuation of the medium property. The $1/Q$ values estimated in many regions of the world are in an approximate range from 10^{-4} to 10^{-1} at frequencies above a few hertz and exhibit a decrease with increasing frequencies (Sato & Fehler 1998). Aki (1980) proposed a method for estimating the $1/Q$ value using the seismic records from a single station. This method can estimate the frequency-dependent $1/Q$ value of the S waves from the spectra of the direct S waves normalized by those in the coda part to eliminate the effects of both the seismic source and site factors. Yoshimoto *et al.* (1993) applied this method to estimate both the $1/Q$ factors for the P- and S waves and evaluated

the frequency-dependent $1/Q$ value in the Kanto area, Japan. Walter *et al.* (2007) developed a method for estimating the apparent attenuation of seismic waves propagating in the crust like Pn, Pg, Sn and Lg waves by using the coda-derived source spectra proposed by Mayeda & Walter (1996). Their methods show similarities with the concept of coda normalization. However, they estimated the source spectra from the energy spectrum in the coda part and then obtained the attenuation factors for the various phases.

The spatial $1/Q$ structures have been examined by using inversion techniques. Tsumura *et al.* (2000) developed a method that inverted the $1/Qp$ values in the spatially distributed blocks, corner frequencies of seismic sources and site responses below the stations from the observed velocity spectra. They assumed the $1/Q$ value to be independent of frequency and applied the inversion method to the northeastern area of Japan. Their results showed that high $1/Q$ regions appear beneath active volcanoes in the upper mantle. According to the methods of Tsumura *et al.* (2000), the $1/Q$ estimation has a resolution of about a few tens of kilometres, and they have assumed that $1/Q$ remains constant with frequency. The attenuation factors at the local scale have been estimated with a high resolution in many areas. Schurr *et al.* (2003) obtained a 3-D $1/Q$ for *P* waves ($1/Qp$) structure for the central Andean subduction zone by means of attenuation tomography using the spectra of direct waves. They discussed the existence of a fluid from the $1/Qp$ value and its spatial distribution based on estimation of the t^* value. t^* is a whole path attenuation operator from the hypocentre to a station, which is a stable parameter that can be used to estimate the attenuation factor. However, the attenuation factor has to be assumed to be frequency independent. Chun *et al.* (1987) proposed a method to estimate Lg-wave attenuation, which eliminated source and site factors by the consideration of the spectral ratio among a pair of stations and a pair of events. They succeeded in obtaining the frequency-dependent attenuation coefficient in the medium between the pair of stations. Blakeslee *et al.* (1989) also utilized a pair of stations and pairs of earthquakes and obtained the spectral ratio to eliminate the source and site factors. Then, they achieved a fine $1/Q$ structure within the San Andreas fault zone, that is, Parkfield. Chun *et al.* (2004) detected a temporal change in the $1/Q$ values for *P* waves at the Loma Prieta rupture zone by carefully analysing the seismograms of the earthquake clusters. In a similar way, many researches have investigated the attenuation structures (e.g. De Lorenzo *et al.* 2001; Peng *et al.* 2003). The key point in the estimation of seismic-wave attenuation is the elimination of the effects of the seismic source, site amplification, etc. In particular, a method for estimating the frequency-dependent $1/Q$ value with high-spatial resolution has to be developed. This dependence of $1/Q$ on frequency can provide information about the spectral structure of the heterogeneity of the medium.

In this study, we propose a new method for $1/Q$ estimation with high resolution, extending to several kilometres, and its applicability to seismic waveforms in an aftershock area of the 2005 West Off Fukuoka Prefecture Earthquake. We also try to determine $1/Q$ of a *P* wave and discuss the relationship between the $1/Q$ structure and various phenomena associated with the earthquake.

The West Off Fukuoka Earthquake (M7.0) on the Japan Meteorological Agency (JMA) scale occurred on 2005 March 20 in the northern part of Kyushu, Japan (referred to as the Fukuoka earthquake). The aftershock distribution of the earthquake and location of the main shock are plotted in Fig. 1. The focal mechanisms of the major aftershocks inferred from the *P* wave first motions in the seismograms are also shown in this figure. On the basis of the aftershock distribution and focal mechanism, the earthquake fault was determined to be a left-lateral strike-slip-type fault with a strike in the WNW–ESE direction (Shimizu *et al.* 2006). The fault strike of the earthquake was almost identical throughout northern Kyushu. An explanation for this strike direction is that the stress field—with the minimum principal axis in the NNW–SSE direction—is present in this region. The principal stress has the same direction as that inferred from the mechanisms of the occurrence of micro-earthquakes in this region (Shimizu *et al.* 2006).

There is an active fault named Kego passing through Fukuoka City along the SE extension of the fault, as shown in Fig. 1. The shear stress on the Kego fault has increased due to the fault motion of main shock because of its relative location to the earthquake fault. To evaluate the interaction between the two faults, the heterogeneous structure in this region needs to be investigated. The seismic activity over a detection limit, which has a magnitude of around 2, was extremely low before the earthquake. For the purpose of improving both the detection limit and accuracy of the event location and studying the aftershock data in a greater detail, temporary seismic stations have been set up by many researchers from different Japanese universities (Shimizu *et al.* 2006). The stations are located both on land and in sea. The collective observations from these stations provided a more accurate distribution of the hypocentre (Uehira *et al.* 2006), particularly in terms of improved accuracy in the determination of the depth of the hypocentre. By using the double-difference (DD) tomography method, Hori *et al.* (2006) estimated the 3-D velocity structures in and around a focal area based on the traveltime data collected during the seismic observations. It was found that the high-velocity regions estimated by inversion are located in the asperity as inferred from the slip distribution. For instance, the coseismic slip distribution of the earthquake (e.g. Asano & Iwata 2006) suggests the existence of heterogeneity of stress and/or strength distribution on the fault. The non-uniform slip distribution requires a mechanism to increase or decrease the stress accumulation due to the slip. The anelasticity of the medium is one of the candidates causing this phenomenon. The post-seismic slip occurring on the earthquake faults was also not spatially uniform (e.g. Nakao *et al.* 2006). The post-seismic slip is possibly related to the relaxation in the medium having an anelastic property. At the same time, the anelasticity would possibly concentrate stress on the fault under the tectonically loaded regional stress field since the anelastic medium can deform prior to the faulting of an earthquake. In this study, we estimate the $1/Q$ distribution and discuss its spatial relationship with seismic activities such as main shock faulting and aftershocks of the earthquake. The relationship between the $1/Q$ distribution and seismic activities will aid in the elucidation of the mechanism of large earthquakes.

METHOD

The purpose of this study is to determine the attenuation structure ($1/Q$) with high resolution using seismograms recorded at a local seismic network. In order to estimate the $1/Q$ structure in the aftershock area of a large earthquake, we improve the coda normalization method of Aki (1980). Coda waves are composed of incoherent scattered waves arriving from many directions to a station (e.g. Aki & Chouet 1975). This feature indicates the low dependence of coda waves on the radiation pattern from a hypocentre, which enables the elimination of both factors of source and average site amplification from the observed spectrum. The coda normalization method utilizes this feature for the estimation of the frequency-dependent $1/Q$ value.

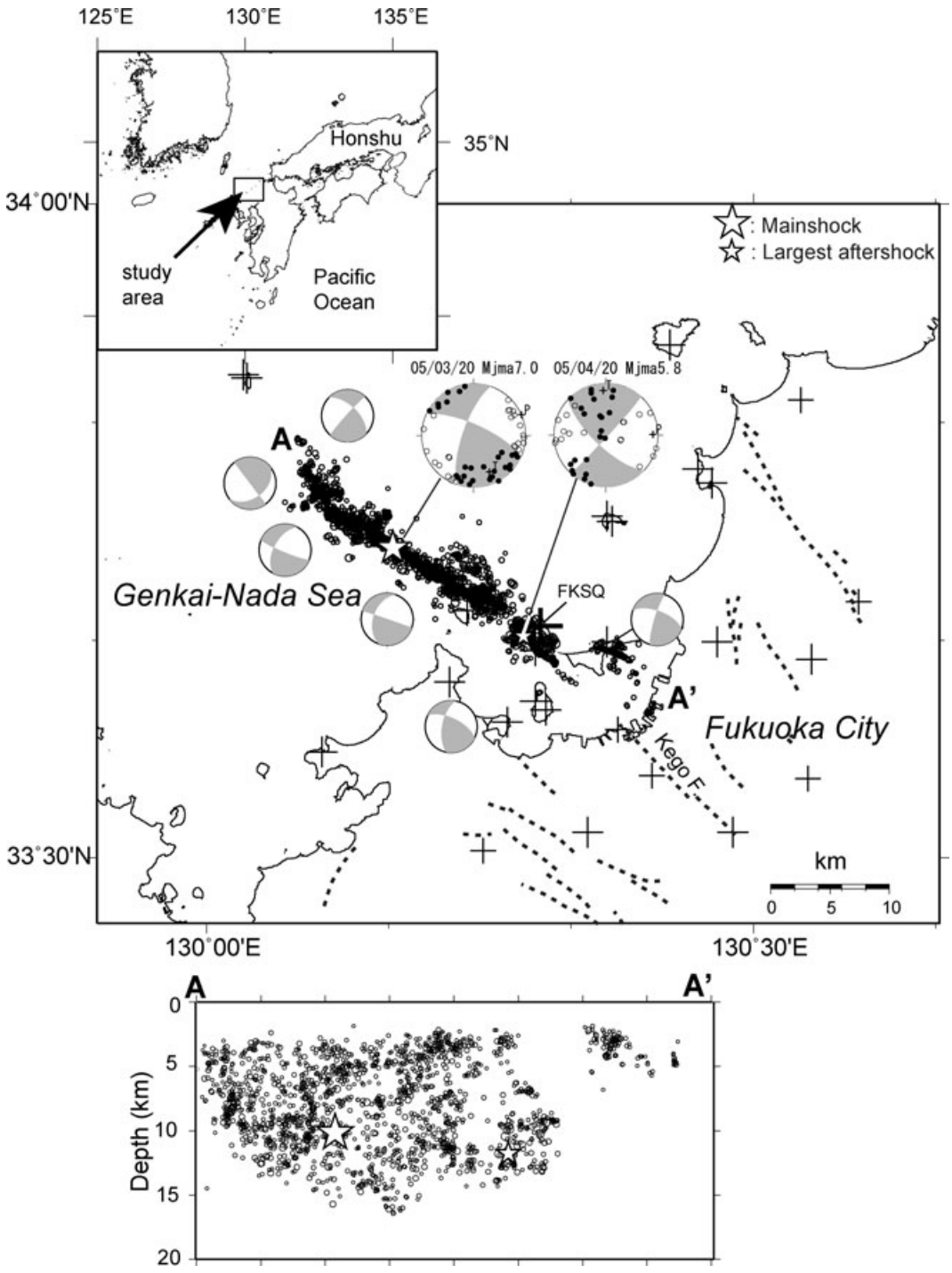

Figure 1. Map showing the distribution of hypocentres (dots) and seismic stations (crosses). The large and small stars denote the hypocentres of the main shock and the largest aftershock, respectively. The focal mechanisms for major events are also displayed by lower hemisphere projection. The lower figure displays a vertical cross-section of the aftershock distribution along line A–A' in the map. The dashed lines indicate active faults including the Kego fault. The cross indicated by 'FKSQ' is the location of the station; examples of waveforms observed at this station are displayed in Fig. 3.

Generally, the power spectrum of the direct wave (Ed_{ij}) for the ith event at the jth station can be expressed as a function of both angular frequency ω and traveltime of the direct wave t_{ij} from the hypocentre of the event to the station

$$Ed_{ij}(\omega, t_{ij}) = \frac{S_i(\omega) I_j(\omega) R_{ij}}{4\pi r_{ij}^2} \exp\left[-\omega Q(\omega)^{-1} t_{ij}\right], \quad (1)$$

where $S_i(\omega)$ is the source power spectrum of the ith event, $I_j(\omega)$ is the station factor including the site effect and instrumental response at the jth station, R_{ij} is the factor of the radiation pattern due to the earthquake source mechanism and r_{ij} is the distance between the source and the station. For a homogeneous velocity structure, the inverse square of r_{ij} represents the geometrical spreading factor. The basic problem in estimating the $1/Q$ value is the elimination of the source, site and instrumental factors.

Generally, the coda energy spectrum can be expressed by the following formula:

$$Ec_{ij}(\omega, t_c, r_{ij}) = S_i(\omega)\overline{I}_j(\omega)C_{ij}(\omega, t_c, r_{ij}), \quad (2)$$

where t_c is the lapsed time at which the spectrum of the coda wave is taken. C_{ij} involves a scattering coefficient and the geometrical factor related to the location of the hypocentre and station. This factor depends on the scattering property of a medium. Two extreme cases showing different scattering properties are considered in the first stage of the study on the scattering problem. These cases are single-scattering and diffusion models for weak and strong scattering properties, respectively. The factor C_{ij} for the models can be written under the assumptions of single scattering (Sato 1977) and diffusion (Aki & Chouet 1975) as follows:

$$C_{ij}(\omega, t_c, r_{ij}) = \frac{g_0}{2\pi V^2 t_c^2} \quad (3)$$

for the single-scattering model ($t_c >> r_{ij}/V$), where g_0 is the scattering coefficient and V is the seismic wave velocity propagating in the medium.

$$C_{ij}(\omega, t_c, r_{ij}) = \frac{1}{(4\pi D_c t_c)^{3/2}} \exp\left(-\frac{r_{ij}^2}{4D_c t_c}\right) \quad (4)$$

for the diffusion model, where D_c is the diffusivity.

In this study, we set t_c such that it is greater than twice the direct S-wave traveltime ($t_c > 2Ts$) for satisfying the condition $t_c >> r_{ij}/V$, proposed by Sato (1977). $\overline{I}_j$ includes both the site factor for the coda wave and the instrumental response at the jth station. The site factor of the coda wave is the average site amplification factor for S waves of rays incident on the station from all directions. Taking the ratio of Ed_{ij} to Ec_{ij}, we get

$$P_{ij}(t_{ij}, \omega) = \frac{Ed_{ij}}{Ec_{ij}} = \frac{\dfrac{S_i(\omega)I_j(\omega)R_{ij}}{4\pi r_{ij}^2}\exp\left[-\omega Q(\omega)^{-1}t_{ij}\right]}{S_i(\omega)\overline{I}_j(\omega)C_{ij}(\omega, t_c, r_{ij})}. \quad (5)$$

The source factor for the ith event is cancelled by this normalization. The coda normalization method of Aki (1980) is used to estimate the $1/Q$ factor at a station (i.e. fixed j) from the lapse time dependence (t_{ij}) of P_{ij} for fixed t_c. The $1/Q$ values for the P and S waves are obtained by substituting direct P- and S-wave energies for Ed in eq. (5), respectively. As suggested by many studies (Sato & Fehler 1998), S-coda waves of natural earthquakes are mainly composed of waves that are radiated as S waves from a seismic source and are scatted by heterogeneity. Therefore, the cancellation of the source factor by the normalization in eq. (5) is valid for $1/Q$ of an S wave since the source factor of the coda wave is same as that in direct waves. On the other hand, in the case of the $1/Q$ estimation of P waves, the spectrum of a direct P wave is normalized by that in the coda part. Coda normalization can be considered for the cancellation of the source spectrum of S waves. The ratio of P-wave source energy to S-wave source energy will not be one, meaning the source effect will remain in P_{ij}. According to the coda normalization method, however, the $1/Q$ value estimation only requires decay rate of P_{ij} with lapse time in eq. (5). Therefore, $1/Q$ of a P wave can be estimated from the ratio data obtained from eq. (5) under the assumption that the energy ratio from the source between the P wave and the S wave is independent of events. The validity of this assumption has already confirmed for small earthquakes by Yoshimoto *et al.* (1993).

Next, we calculate the ratio of P_{ij} for the ith event to $P_{i'j}$ for the i'th event at the same station j. If the location of the ith event is close to that of i'th event, then the ratio (X) can be simplified as follows:

$$\begin{aligned} X_{ii'j}(t_{ij}, t_{i'j}, \omega) &= \frac{P_{ij}(t, \omega)}{P_{i'j}(t, \omega)} \\ &= \frac{\frac{I_j(\omega)R_{ij}}{4\pi r_{ij}^2}\exp\left[-\omega Q(\omega)^{-1}t_{ij}\right]}{\overline{I}_j(\omega)C_{ij}(\omega, t_c)} \Bigg/ \frac{\frac{I_j(\omega)R_{i'j}}{4\pi r_{i'j}^2}\exp\left[-\omega Q(\omega)^{-1}t_{i'j}\right]}{\overline{I}_j(\omega)C_{i'j}(\omega, t_c)} \\ &\approx \frac{R_{ij}r_{i'j}^2}{R_{i'j}r_{ij}^2}\exp\left[-\omega Q(\omega)^{-1}(t_{ij} - t_{i'j})\right] \\ &\because\ C_{ij}(\omega, t_c) \approx C_{i'j}(\omega, t_c). \end{aligned} \quad (6)$$

In the above formula, t_c for P_{ij} is identical to that for $P_{i'j}$. Using a fixed lapse time for recording the coda spectrum for different events yields similar scattering shells for the two event; scattering shells for two events are schematically shown in Fig. 2. In such a case, C_{ij} is cancelled by $C_{i'j}$. However, this assumption will not be valid in the case of a large difference between the C factors determined by the scattering shells. For instance, the C value depends on the hypocentral distance even in a medium with a uniform scattering property. The difference between the coda energies of an event pair can be calculated from the scattering model (i.e. single scattering and diffusion). Based on the two models described previously, we can verify the reliability of this cancellation. The expected difference between the C values estimated for practical event-pair combinations used in this analysis (described in the following sections) is less than 1 per cent for both the models involving single scattering and diffusion. Therefore, the cancellation of the coda factor is sufficiently reliable in our practical analysis.

In the same way, the site factors of the coda waves are eliminated from eq. (6). The ray path for a direct P wave of the ith event is almost the same as that of the i'th event since the difference between both the locations of the events is assumed to be small. Under this condition, I_{ij} is cancelled by $I_{i'j}$. In addition, $1/Q$ in eq. (6) is only influenced by the medium adjacent to the events. Taking the logarithm of eq. (6) and dividing by the angular frequency, we obtain

$$\begin{aligned} X'_{ii'j} &\equiv \ln\left[X(t_{ij}, t_{i'j}, \omega)\right]/\omega \\ &= \ln\left(\frac{R_{ij}r_{i'j}^2}{R_{i'j}r_{ij}^2}\right) \Bigg/ \omega - Q(\omega)^{-1}\Delta t_{ij},\ \Delta t_{ii'j} = t_{ij} - t_{i'j}. \end{aligned} \quad (7)$$

Note that the X' value for an event pair is affected by $1/Q$ of the medium between the event pair. It does not depend on the station location as long as the ray paths are assumed to be similar. The above equation suggests that $1/Q$ can be estimated from the linear variation of X' with the traveltime difference $\Delta t_{ii'j}$. X' can be obtained for each i–i'–j combination. We perform the spectral analysis for many events and stations based on eqs (5)–(7). Then we get the X' data set of the event-station pairs. The frequency-dependent $1/Q$ values are obtained from the X' data for different frequency bands. This concept is similar to the DD hypocentre determination method proposed by Waldhauser & Ellsworth (2000) and the DD tomography method proposed by Zhang & Thurber (2003) for velocity estimation. Consequently, we obtain the $1/Q$ value in the hypocentral area by taking the DD in the logarithmic power spectra of an adjacent event pair.

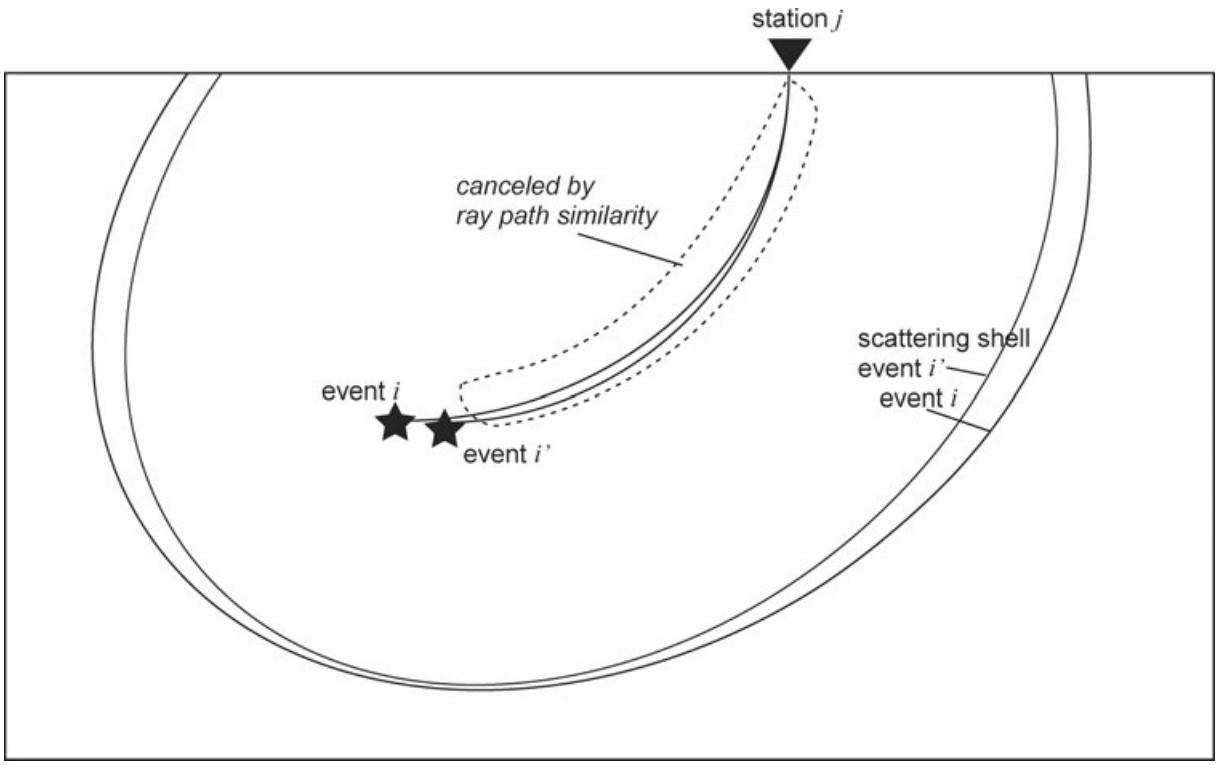

Figure 2. Schematic illustration of the coda normalization method for an event pair. For a fixed lapse time (t_c), the scattering shells of two adjacent events share almost the same region.

DATA AND ANALYSIS FOR 1/*Q* ESTIMATION OF *P* WAVES

In this study, we estimate the 1/*Q* structure of a *P* wave in the aftershock area of the Fukuoka earthquake. A waveform analysis is applied to the data recorded at temporal stations deployed after the main shock occurrence and at the stations set up by JMA, the National Research Institute of Earth Science and Disaster Prevention (Hi-net) and Kyushu University. The locations of these stations are shown in Fig. 1. We relocate the hypocentres of the earthquakes that occurred from 2005 March 20 to May 31 based on the 3-D velocity structure (Hori *et al.* 2006) using the DD tomography program developed by Zhang & Thurber (2003) for fixed-velocity structures. The relocated hypocentres are plotted (indicated by circles) in Fig. 1. Since the earthquakes employed in the present analysis occurred from 2005 March 21 to May 31, the temporal observation sites deployed during this period enabled the determination of the hypocentres with high accuracy. The total number of earthquakes analysed is 1781. The magnitude range used in the analysis is from 1.9 to 5.1. The accuracy of hypocentre determination is less than 0.005° along the horizontal direction and less than 0.5 km in depth. The focal mechanisms were determined for 186 events among the earthquakes used in this study from the polarity data of the first *P*-wave arrival obtained from more than 30 stations.

Examples of waveforms observed at the seismic station FKSQ are shown in Fig. 3. To obtain the spectral ratio data (X'), we follow the sequence of processing shown in Fig. 4. We only analyse the seismograms with a signal-to-noise ratio of greater than 2 in the coda part. The power spectrum of the direct *P* wave is calculated for 0.5 s from its arrival time in the vertical component of the seismogram. The spectral time window is cosine tapered at both the edges. Taking spectral ratio requires that both spectra of a numerator and denominator of the ratio are calculated from data with same time window length. Therefore, the spectrum in the coda part is estimated from the data extracted from the vertical component seismogram by the time window that is from a lapse time larger than twice the direct *S*-wave traveltime (*2Ts*) for 0.5 s. In this analysis, the spectrum in the coda part is averaged for about 10–16 spectra that are acquired in different coda parts after *2Ts* in order to stabilize them. The extracted data is from the seismogram with lapse time of *2Ts–Tn*, where *Tn* is a lapse time at which amplitude of waveform is equal to twice of noise level. In other words, the spectrum in the coda part is taken from the time window with a length of 5–8 s. The time window length is *Tn–2Ts*. The extracted data is divided into small time windows with lengths of 0.5 s. Then, the spectra are calculated for small time windows and then averaged. Fig. 3 also shows an example of the spectra for a direct *P* wave, a coda wave and noise.

The direct *P*-wave spectrum is affected by the radiation pattern from the hypocentre, as shown in eq. (5). The direct *P*-wave amplitude radiated near the nodal planes of the source becomes small. On the other hand, the *P*-coda wave, which appears as a wavelet between the direct *P*-wave arrival and the *S*-wave arrival, has a certain amplitude at any time and is independent of the focal mechanism. Therefore, the small amplitude observed at and around the direct *P*-wave arrival can be attributed largely to the *P*-coda wave, and not the direct *P* wave. We will overestimate the direct *P*-wave energy if *P*-coda wave is larger than direct *P*-wave energy. The origin of the *P*-coda wave has been discussed in many studies (e.g. Kuwahara *et al.* 1997; Wagner 1998). In this study, however, we do not consider the effect of the *P*-coda wave for simplicity. To prevent the interference of *P*-coda energy and the direct *P*-wave energy, we adopt only the data of the direct *P* wave, the energy of which is four times higher than the average energy of the *P*-coda part. For the

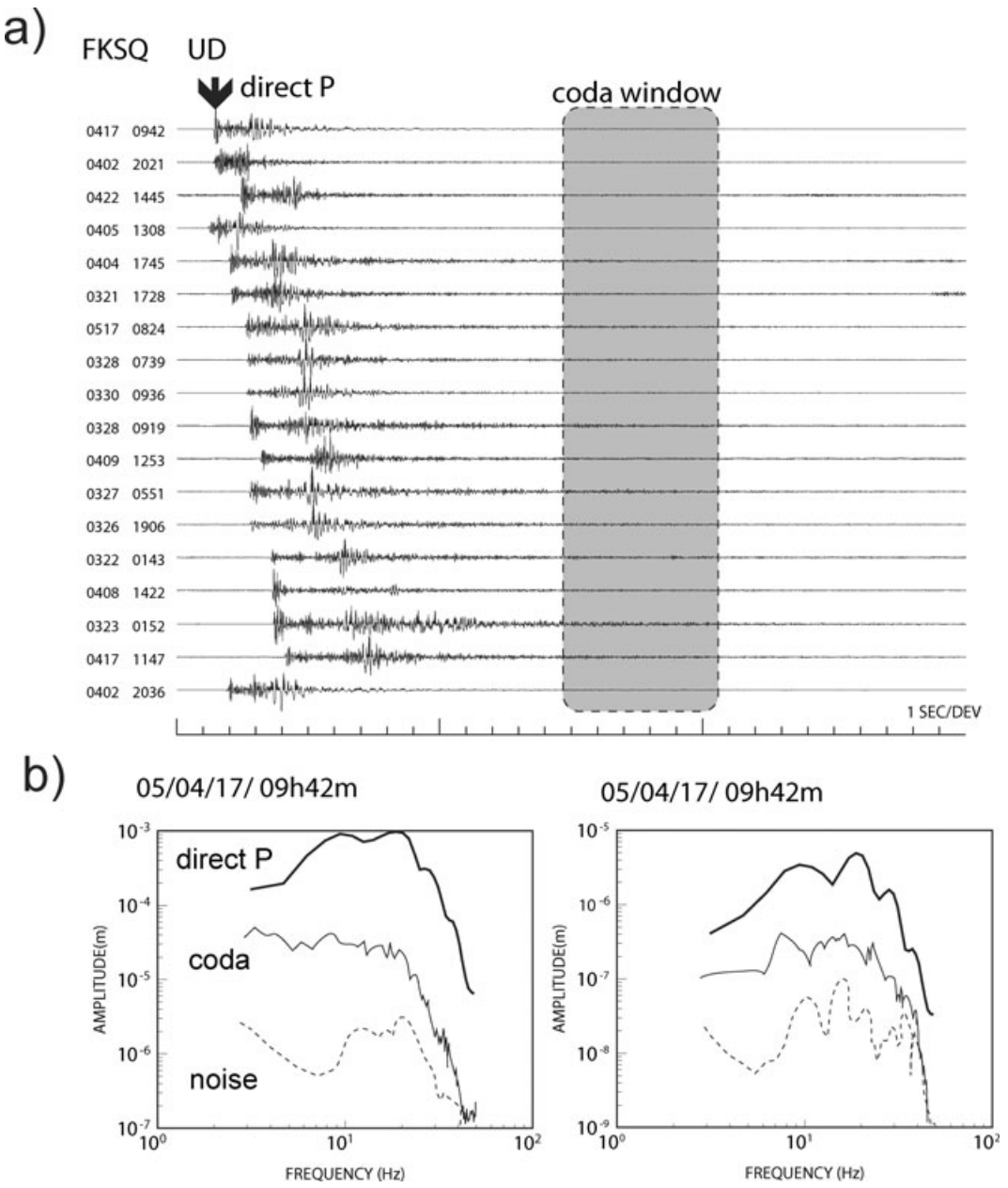

Figure 3. Top panel: examples of waveforms observed at FKSQ. The seismograms displayed are the recordings of the aftershocks along the vertical component. The hatched area shows the time window used to obtain the spectrum for the coda waves. Bottom panel: examples of the spectra for the direct *P* wave, coda wave and noise. A power spectrum with signal-to-noise ratio greater than 4 is adopted. Frequency ranges used for the $1/Q$ estimation are 0–5, 5–10, 10–15, 15–20, 20–25, 25–30, 30–35 and 35–40 Hz.

waveforms satisfying this criterion, the ratios of the direct *P*-wave spectrum to the coda spectrum (*P* in eq. (5)) are calculated.

Next, we calculate the ratio X from the *P*-values for two adjacent events at the same station [i.e. X in eq. (6)]. The coda spectra of the event pairs are calculated using identical lapse time windows, which are affected by inhomogeneities distributed in similar spatial regions. We eliminate the pairs for which the distance between the event pair is greater than 10 km for maintaining the spatial resolution. The range of Δt adopted in this study does not only limit the measurement of decay in $1/Q$ estimation (eq. 3) but also controls the spatial resolution since the $1/Q$ estimation assumes a uniform $1/Q$ structure between the event pairs. We adopt the event pairs with a distance greater than the location error of the hypocentre, so that the X' data with Δt less than 0.1 s is eliminated to prevent the introduction of the estimation error caused by the uncertainty in hypocentre determination. We determine the $1/Q$ value for event pairs and stations from the X' values (obtained from X) by least-squares fitting eq. (3). We divide the X' data into eight frequency ranges, namely the bands of 0–5, 5–10, 10–15, 15–20, 20–25, 25–30, 30–35 and 35–40 Hz.

We adopt another criterion for event-pair selection in order to maintain the ray path similarity between the event pairs to obtain the ratio X. If the two events are located on identical ray paths from the station to the event pair, the $1/Q$ value is correctly obtained from the attenuation of their power spectrum with a traveltime difference between the two events. However, if the distance between

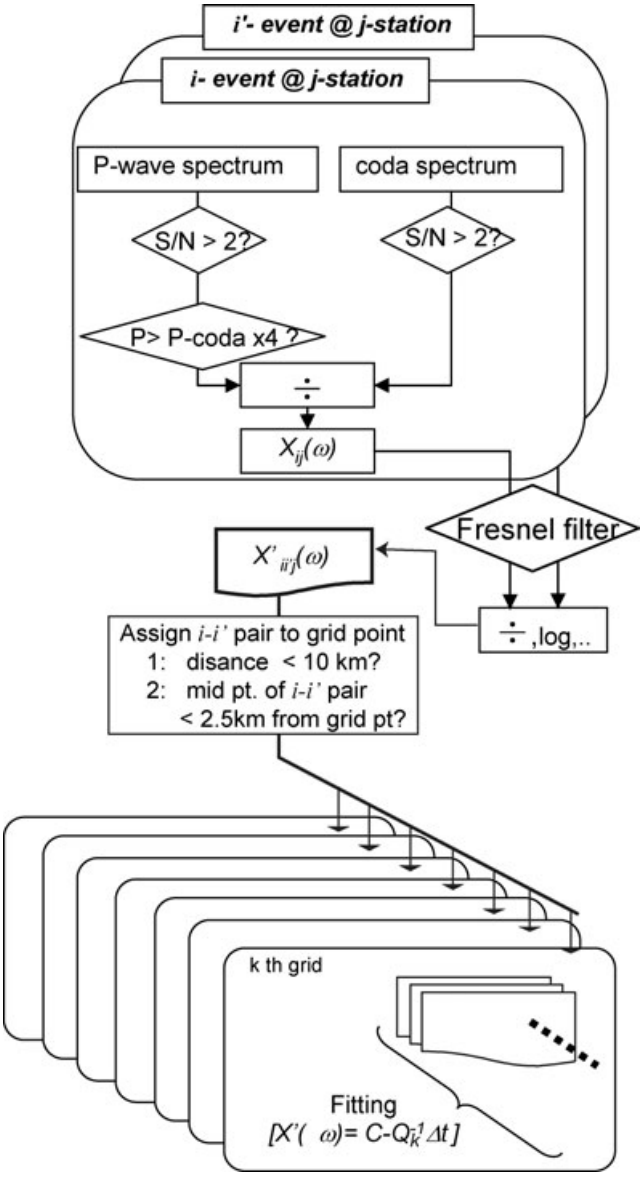

Figure 4. Block diagram for $1/Q$ estimation. The processing sequence for estimating X' for a pair of ith and i'th events at the jth station is displayed. The $1/Q$ values can be estimated by measuring many X' corrected for every event pair obtained from the stations of the seismic network.

the events is large even for small traveltime differences (i.e. small Δt), the $1/Q$ value in the region between these events is inaccurately estimated. In this case, the estimated $1/Q$ value is the average $1/Q$ value in an area where the rays of the event pairs travel. Here, we adopt a Fresnel zone limit for checking the ray path similarity. Let us consider an event pair. If an event (ev. 1) of the pair having its ray length shorter than that of the other one (ev. 2) is located in the 1st Fresnel zone of the ray path of ev. 2, we use the data from this pair for estimating the $1/Q$ value at a grid. The 1st Fresnel zone radius r_f is defined as

$$r_f = \sqrt{\lambda \frac{d_1 d_2}{d_1 + d_2}}, \tag{8}$$

where λ is the wavelength. Here, d_1 and d_2 are the distances to ev. 1 from the hypocentre of ev. 2 and station, respectively. In this study, we use the approximate distance along the ray path in the 3-D velocity structure as d_1 and d_2. A schematic illustration of the Fresnel zone size and its relationship with event selection is shown in Fig. 5. Generally, any ray path travelling within the same Fresnel zone cannot identify the differences in the structure along the paths. It means that the Fresnel zone size can be used to determine the resolution limit on the basis of the wave propagation theory. Therefore, this limit is a sufficient condition to determine the ray path similarity. For example, the radius of the 1st Fresnel zone is less than 2 km in the case of $d_1 = d_2 = 10$ km and $\lambda = 0.6$ km. We perform 3-D ray tracing using the velocity structure estimated in this region and check the ray paths for the event pairs. After getting ray path of the ev. 2, we calculate the length of the segment normal to the ray path from the location of ev. 1. In case the calculated length is less than 1st Fresnel zone radius at the cross point between the segment and the ray path, we adopt the data of this event pair to calculate the ratio ($X_{ii'j}$).

In order to solve eq. (7) and to obtain the $1/Q$ value, we should know the value of the geometrical spreading factors for the event pairs. We verified the effect of the geometrical spreading factors based on the 3-D velocity structure obtained by Hori *et al.* (2006). The factor for the inhomogeneous velocity model deviated by less than 10 per cent as compared to that for the homogeneous one. Therefore, the distance between the hypocentre and the station is adopted as the geometrical spreading factor, expressed by eq. (3), for simplicity. The effect of the radiation pattern should also be known *a priori* since for a given pair, this effect can change the offset value of X' in the regression analysis employing Δt. The effects are corrected by the focal mechanisms for 186 events. Most of the mechanisms are strike slips with the compression axis (pressure axis) along the WSW direction and the tension axis along the SSE direction. Fig. 6 shows the histograms of the determined directions of the compression and tension axes. The X' value for a pair composed of data from the events with well-determined focal mechanisms is corrected with its radiation pattern factor, except for a single case wherein a wave with a small amplitude is radiated near a nodal plane at the hypocentre. This small amplitude provides large correction in the X' value. Therefore, the correction can have a large error even if the estimation error for the focal mechanism is small. We do not adopt the focal mechanism correction for the X' value whenever the radiated amplitude calculated by the focal mechanism is less than 0.2. The lower limit of 0.2 is based on the event selection method mentioned earlier. We have eliminated the data of the direct P wave with amplitudes smaller than twice the amplitude in the P-coda part. The maximum P-wave amplitude in our dataset is about 10 times greater than that in the P-coda part. If the P wave with the maximum amplitude is assumed to be radiated from the direction of either the compression or tension axis, the magnitude of the radiation pattern effect would be 1.0. Then, the criterion of event selection could maintain the magnitude of the effect of the radiation pattern to be greater than at least 0.2. For most earthquakes, we could not determine the focal mechanisms with sufficient accuracy. Aki (1980) assumed that the effect of the radiation pattern can be smoothened out by considering a sufficiently large number of earthquakes. In this study, we use the X' value for many event pairs and stations. These data can smoothen out the effect of the radiation pattern. On the other hand, the $1/Q$ value is also obtained from the X' data in a narrow Δt range (i.e. 0.1–1.8 s) when the event pairs are selected from a small cluster of earthquakes. The narrow range induces uncertainty in the estimation. The pressure and tension axes of the focal mechanism do not yield a uniformly random distribution, although a Gaussian distribution is observed around the average values (Fig. 6). This suggests a possibility of

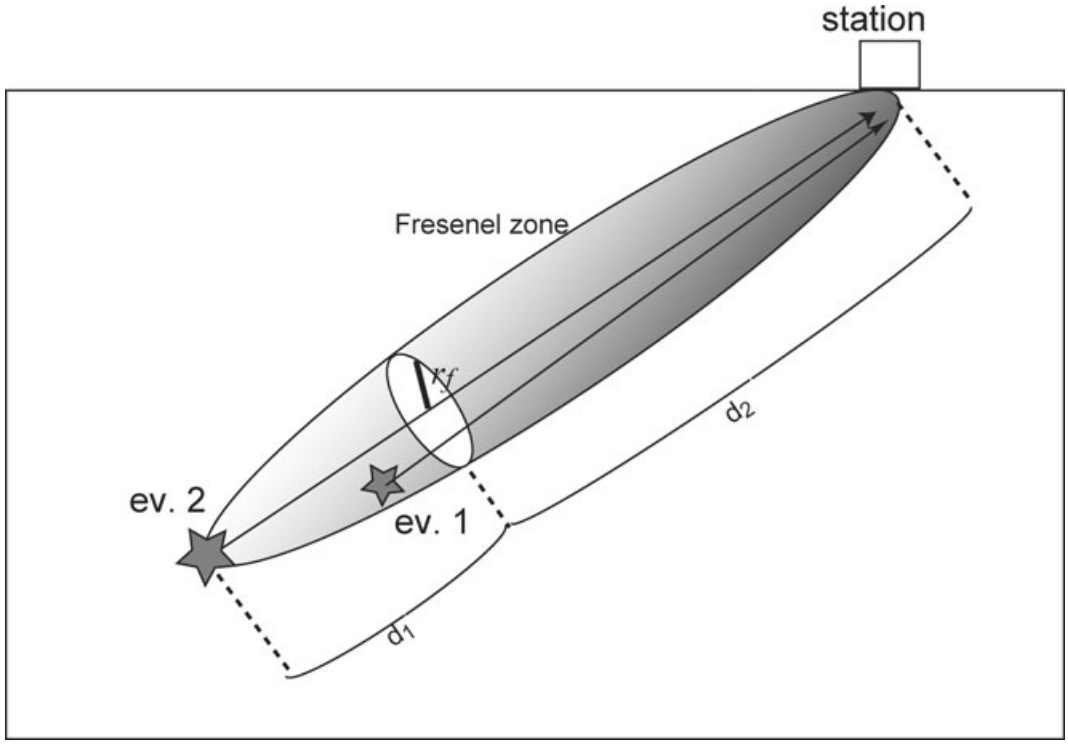

Figure 5. Schematic illustration of Fresnel zone size and its relationship with event selection.

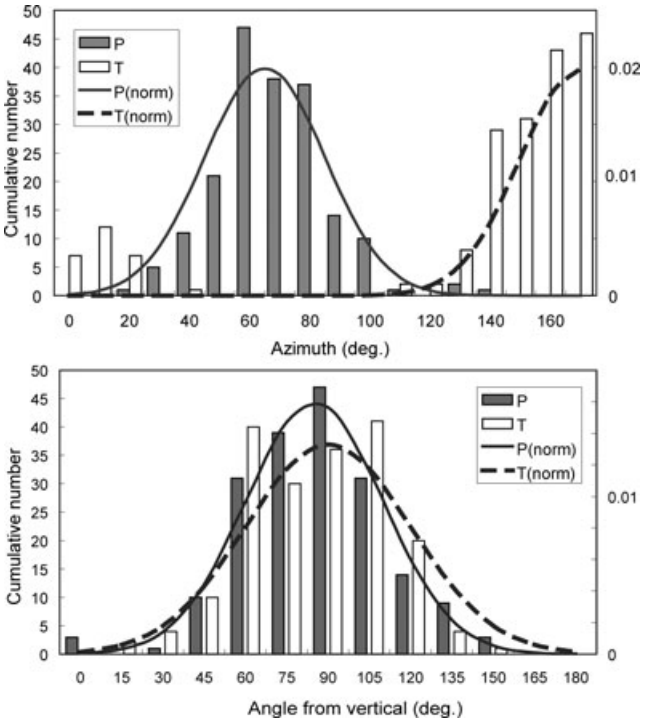

Figure 6. Histograms of the pressure axes of the focal mechanism. The top and bottom diagrams show the cumulative number of earthquakes at the azimuth and an angle from the vertical, respectively. The solid and open bars indicate frequencies of the axes of pressure (P) and tension (T), respectively. The Gaussian probability density functions fitted to the frequency distribution are displayed by the solid (P) and dashed (T) lines.

observing a systematic trend in the X' distribution. In order to suppress the effects relating to the undetermined radiation pattern, X' is corrected by the radiation pattern based on the focal mechanism having the averaged directions of the compression and tension axes.

The $1/Q$ values are estimated at the spatially distributed gridpoints, as shown in Fig. 7. The gridpoints are located in the aftershock region at 5-km intervals along the horizontal and depth directions. This setting assumes a homogeneous $1/Q$ structure around the gridpoint for a resolution of 5 km. The maximum distance of an event pair has lower resolution than that set by the gridpoint interval used for the stable estimation of the $1/Q$ value. We can set the 3-D gridpoints to obtain the structure along a direction perpendicular to the aftershock alignment. However, most of the aftershocks occurred around the fault plane of the Fukuoka earthquake, which means that the $1/Q$ estimation has lesser resolution in the direction normal to the fault plane. The $1/Q$ value at a gridpoint is obtained from the selected X' data such that the midpoint of the event pair is located at a distance of less than 2.5 km from the gridpoint in a direction parallel to the fault. This selection yields a 2-D $1/Q$ structure (i.e. parallel to the fault and depth directions) in this study.

RESULTS

By means of the abovementioned pre-processing, we prepare the data set for the $1/Q$ estimation for every frequency band. Then, we estimate the $1/Q$ value by the linear least-squares method with nonnegative constraints (Menke 1989) since the $1/Q$ value must be positive under our assumption. In this study, the $1/Q$ value is estimated independently at each gridpoint. Each bin in Fig. 8 shows the X' variations with Δt at spatially distributed gridpoints. In this figure, the X' values plotted are corrected by either a well-determined focal mechanism or an average focal mechanism. Each graph of X'—Δt is placed on the gridpoint put on the location of the relative

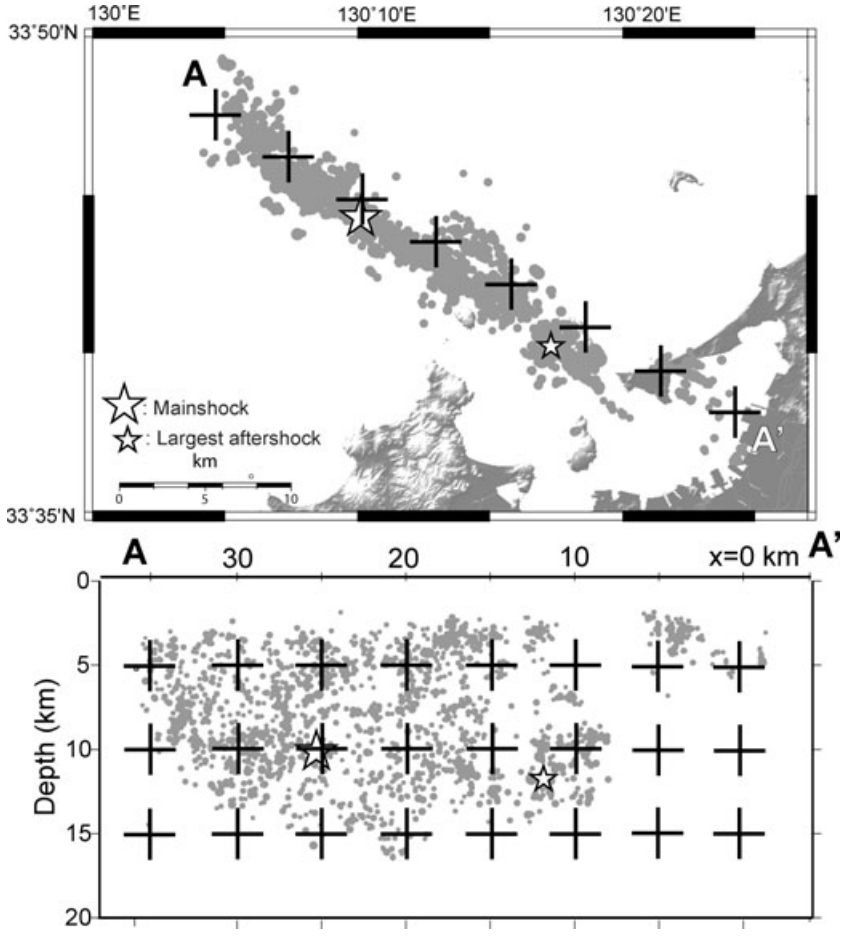

Figure 7. Grid distribution for estimating $1/Q$. The $1/Q$ value is estimated at each gridpoint. An event pair for which the midpoint is closer than 2.5 km off from a gridpoint is adopted for the estimation at the grid. The location of the gridpoint is expressed by (x, z), where x is the horizontal distance along the northwest and z is the depth.

grid projected onto the vertical cross-section of the fault. The decay rate of the X' value is equal to the $1/Q$ value, which is indicated by the red line in each graph calculated from the optimum solution in the least-squares estimation. The number of data values (N) used in the estimation is small for a higher-frequency range because of not only the relatively low signal-to-noise ratio but also the small Fresnel zone size. The $1/Q$ estimation error [d($1/Q$)] decreases with increasing N. We discuss the spatial distribution of the $1/Q$ value for $N > 100$ and for errors smaller than either the estimated value or 0.0025. All the selected results based on these criteria are plotted in Fig. 9. It can be observed that the estimated $1/Q$ values are in a range below 10^{-1} and show a decrease with increasing frequency. This

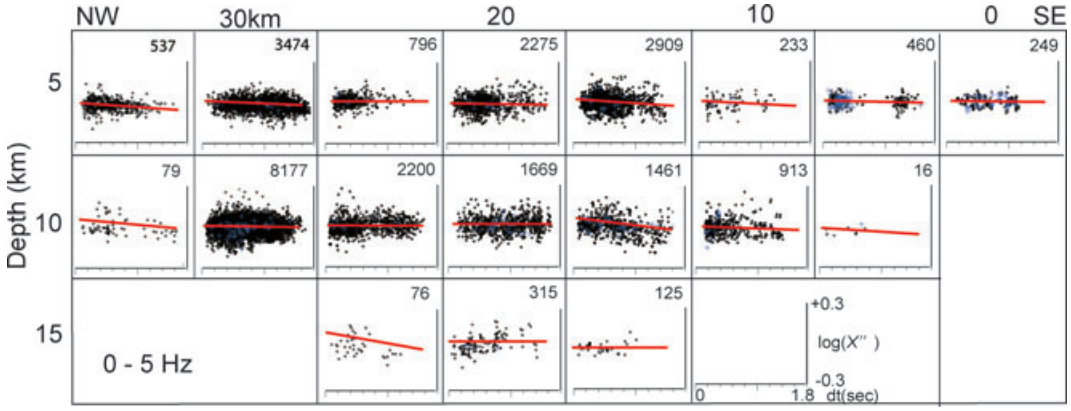

Figure 8. X' variation in Δt for each frequency range. The graph of variation at each gridpoint is placed on the location of the grid in the vertical cross-section along the grid distribution. The blue crosses and dots show X' with and without correction for the radiation pattern, respectively. The red line indicates the solution obtained by fitting the data to eq. (3). The numeral above the variation indicates the number of data values used in the estimation. The number of X' values with the correction is mentioned in the parentheses.

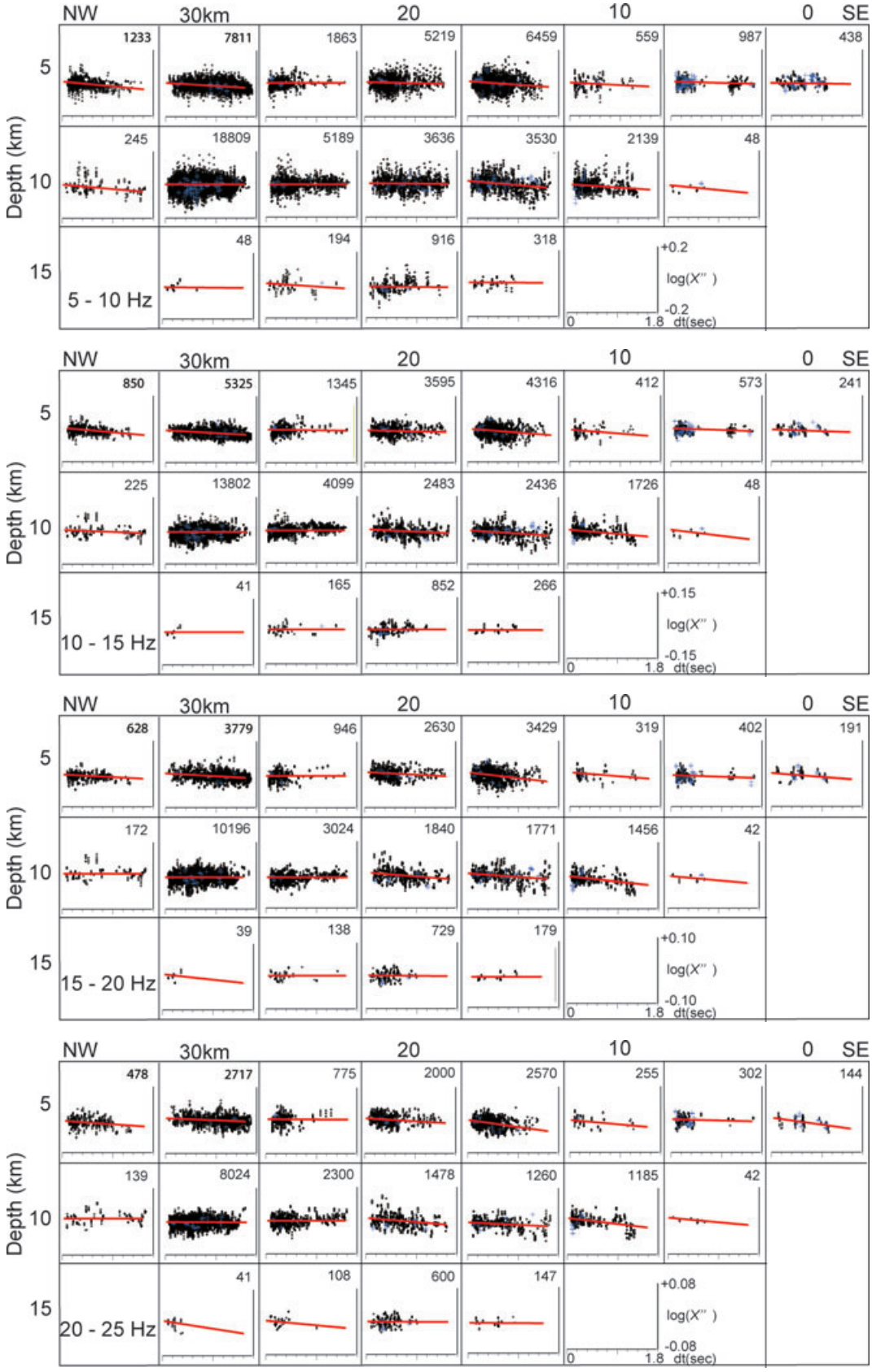

Figure 8. *(Continued).*

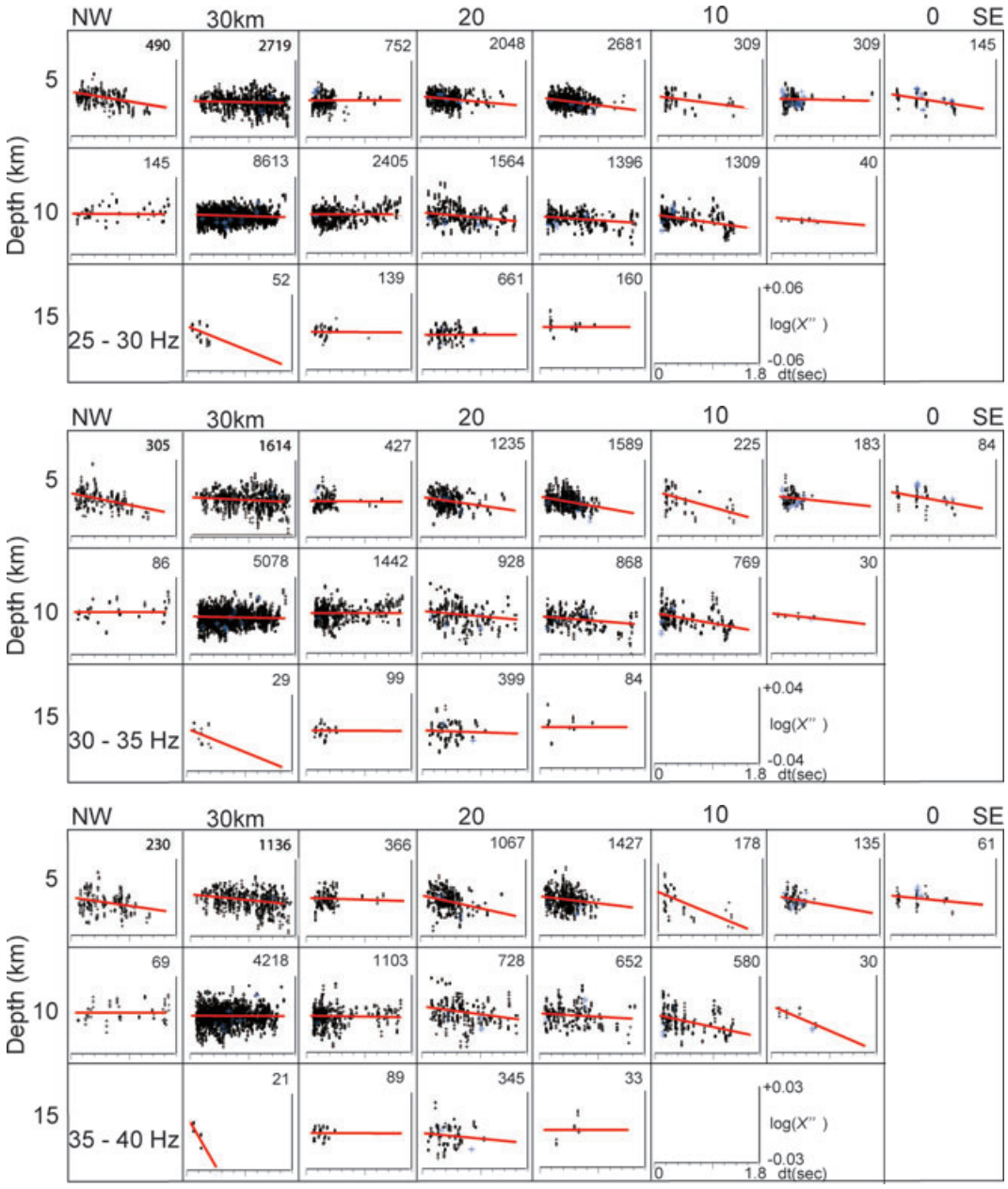

Figure 8. *(Continued).*

frequency dependence can be expressed as a power of frequency, that is $1/Q = 0.02f^{-0.3}$, by fitting an autoregression curve to the estimated $1/Q$ values greater than 0.0025. The $1/Q$ values at several gridpoints become zero, which means that the X' decay rate is too small to be estimated using this method. We selected a $1/Q$ value estimated using an error smaller than 0.0025, which implies that an absolute value smaller than 0.0025 and its frequency dependence are inconsequential. The grey line in this figure indicates the frequency variation of the $1/Q$ values at each gridpoint. The maximum frequency dependence is –1.2 at the gridpoint $(x, z) =$ (15, 10 km). The $1/Q$ value shows a small dependence of less than 0.1 at (10, 5 km). The dependence is different for different gridpoints, which is an advantage of this method since the $1/Q$ value is estimated independent of both frequency and gridpoint. Although the $1/Q$ value decreases with increasing frequency, in general, it is difficult to discuss its spatial variation due to the large fitting error. In this study, unfortunately, we only discuss the spatial variation of $1/Q$.

To obtain the spatial variation of the $1/Q$ structure, we spatially interpolate the $1/Q$ values at the grids by using GMT gridding software which can calculate an interpolated surface of data with adjustable tension continuous curvature from randomly distributed data points (Smith & Wessel 1990). After this processing, we obtain the spatial distribution of the $1/Q$ value for each frequency band, as shown in Fig. 10. The results in this figure show that the low $1/Q$ values are distributed in the middle part of the fault plane. It should be noted that high $1/Q$ regions exist at the edges of the fault plane (i.e. the southeastern and northwestern parts). To put it concretely, low $1/Q$ values appear at $(x, z) =$ (25, 5 km) and (25, 10 km) in all frequency ranges. At (10, 10 km), the $1/Q$ values become high at frequencies higher than 7.5 Hz. A high $1/Q$ region is found at (15, 10 km) until 7.5 Hz. In addition, $1/Q$ is relatively high at

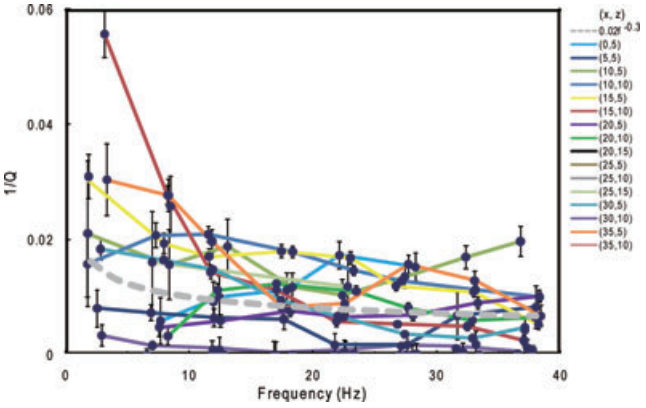

Figure 9. Plot of the obtained $1/Q$ values. The vertical bar (solid circle) denotes the estimation error. The grey dashed curve shows the regression curve fitting to the results and is expressed by $1/Q = 0.02f^{-0.3}$, where f is the frequency. Colour line connecting solid circles denotes $1/Q$ values for each gridpoint which location (x, z in km) is indicated in the right of the figure.

(35, 5 km) although at 17.5 Hz, $1/Q$ is not significant. General features of relative $1/Q$ appearing in all the frequency bands seem to be similar about the spatial pattern of the distribution.

DISCUSSIONS

For estimating $1/Q$ of a P wave using this method, we have to consider the effect of the difference between the source spectra for the P and S waves as described previously. Let us consider the source effect, which should be removed by normalization (P in eq. 1), the ratio between source spectra of P and S waves can be written as

$$\bar{S}_i(\omega) = S_i^P(\omega) \big/ S_i^S(\omega), \tag{9}$$

where S^P and S^S are the source spectra for the P and S waves, respectively. Generally, this factor assumes a constant value except in the range between both corner frequencies for the P and S waves. In this study, we also obtain the ratio between the adjacent events, as given by eq. (6). More strictly, the source effect in the term $X_{ii'j}$ can be written as

$$X_{ii'j}(t_{ij}, t_{i'j}, \omega) \approx \frac{R_{ij} r_{i'j}^2}{R_{i'j} r_{ij}^2} \exp\left[-\omega Q(\omega)^{-1}(t_{ij} - t_{i'j})\right] \frac{\bar{S}_i(\omega)}{\bar{S}_{i'}(\omega)}. \tag{10}$$

The error in estimating the $1/Q$ value will occur in case the ratio $(\bar{S}_i/\bar{S}_i')$ is not equal to 1. In case the corner frequencies of an event pair are the same, this ratio becomes 1. However, this ratio varies at around the corner frequencies for two events if the corner frequency of an event is different from the other event. In other words, this ratio depends on the difference between the earthquake magnitudes of the event pair. According to the observational study carried out by Rautian *et al.* (1978), this ratio is constant at lower frequencies as compared to at the corner frequencies of earthquakes. On the other hand, the ratio (S^p/S^s) increases with frequency at higher-frequency ranges as compared to the corner frequencies. They showed that the behaviour of the ratio for many earthquakes is similar and is independent of spectral shape of the earthquakes. Yoshimoto *et al.* (1993) have estimated $1/Q$ of P waves by the coda normalization method by analysing spectra in a narrow magnitude range. Let us consider the ratio between large and small earthquakes. In a frequency band, the corner frequencies are higher than the analysed frequency for small events. On the other hand, the corner frequencies are lower than the analysed frequency for large events. There is a possibility that the ratio $\ln(X_{ii'j})$ might be biased because of the difference between the ratios of two events. The bias of $\ln(X_{ii'j})$ of the large earthquake to small one will be reverse of the bias of the small earthquake to the large one. The bias will be cancelled if the location of the event is random. Therefore, the decay rate of $\ln(X)$ can can be the $1/Q$ value if we consider many stations and take a variable combination of events. This cancellation will also take place if the source spectra of events are different. Therefore, we can conclude that no systematic error appears in this estimation. A theoretical approach is used to estimate the Sp/Ss value in the higher-frequency range. In the case of the ω^2 model for a seismic source spectrum (Sato & Hirasawa 1973), the ratio at higher frequencies is higher than that at the corner frequencies. Then, $X_{ii'j}$ will be factor two in largest case. The maximum deviation is less than a factor of 2 [i.e. $\pm\ln(2)/\omega$ in eq. (3)]. This effect does not induce large errors as observed in the case of X' dependence of Δt (Fig. 8). In addition to this, the abovementioned averaging effect caused by the random distribution of hypocentres with various magnitudes eliminates perturbations. We showed the magnitude difference in event pair in Fig. 11. The difference is calculated by subtracting magnitude of the farer event of the pair from the nearer one. We can see the average is zero and the distribution does not bias. This means that the cancellation described above is reliable in this study. Therefore, we ignore this effect in this study.

Here, we would like to consider the possible errors the $1/Q$ estimation and the physical meaning of the estimated $1/Q$ values. The $1/Q$ value obtained from the direct wave is a combination of the effects of both intrinsic and scattering attenuations. However, it is difficult to separate these attenuations in the present case. Fehler *et al.* (1992) have developed a method based on the radiative transfer theory to estimate the composition of the $1/Q$ value. Hoshiba (1993) enabled to apply this separation to the data from single station. These methods can discriminate the intrinsic effect from the scattering one by performing a waveform analysis using a large time window. Thus, the low spatial resolution is unavoidable. In this study, we decided the spatial resolution takes precedence over the separation between intrinsic and scattering factor. As another factor, there is a possibility that the estimated $1/Q$ factors are affected by inadequate correction of the geometrical spreading factor. We assumed the factor is inverse of the travel distance of the direct wave. Although we have confirmed the discrepancy in the factors of the 3-D velocity structure, an error in the evaluation of the factor affects the correct estimation of the absolute $1/Q$ value. For instance, let us consider a wave propagating in media with extremely low velocity structures such as fracture zones on faults, which the low velocity zone cannot be detected by tomographic velocity inversion method. In this case, the estimated $1/Q$ value contains not only the attenuation effect due to $1/Q$ but also the energy loss due to trapped waves in the fracture zone. There is a possibility of temporal change in the faulting plane of the earthquake. This also results in an error in the present estimation since we have assumed that $1/Q$ does not vary during the period of the analysis. However, the resolution of the estimation method is so low that such a change in the fault plane cannot be detected. We estimated the $1/Q$ value not in the fault plane, but in the aftershock area. The $1/Q$ change in the fracture zone of the earthquake could not be detected in our estimation because the zone was probably too narrow. Since the resolutions of this

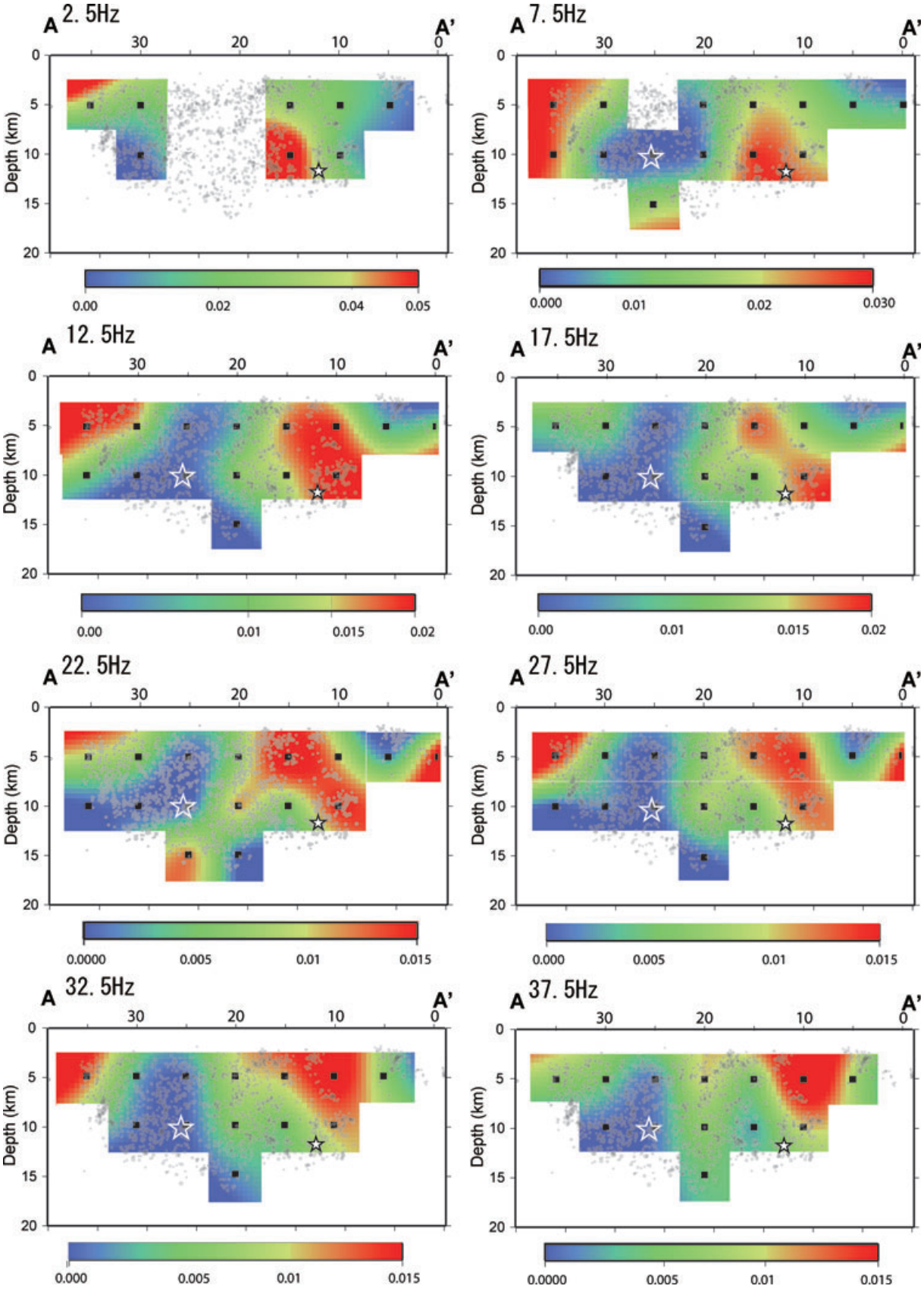

Figure 10. Vertical cross-section of $1/Q$. The $1/Q$ distribution is obtained by interpolating the results at the gridpoints. The large and small stars denote the hypocentres of the main shocks and largest aftershocks, respectively. The solid square is the gridpoint where a reliable solution has been obtained in the estimation. The grey dot indicates the location of the aftershocks.

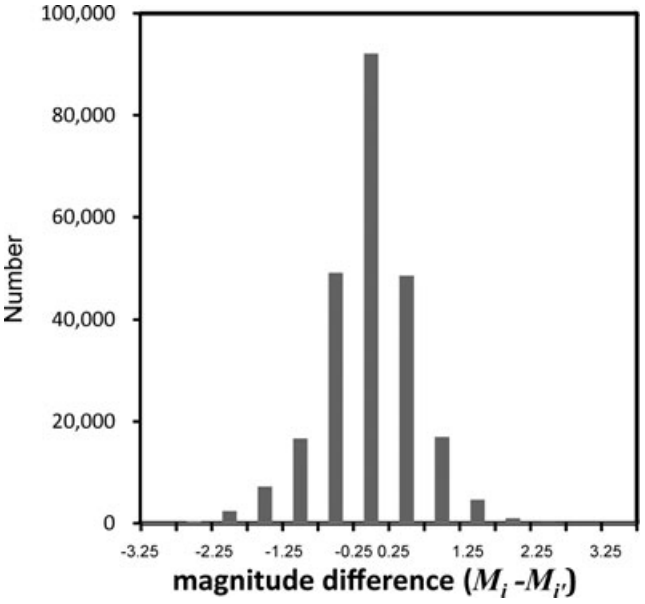

Figure 11. Frequency distribution of magnitude difference in event pairs used in this study. The difference is compared the magnitude of nearer event to station with that of farther one.

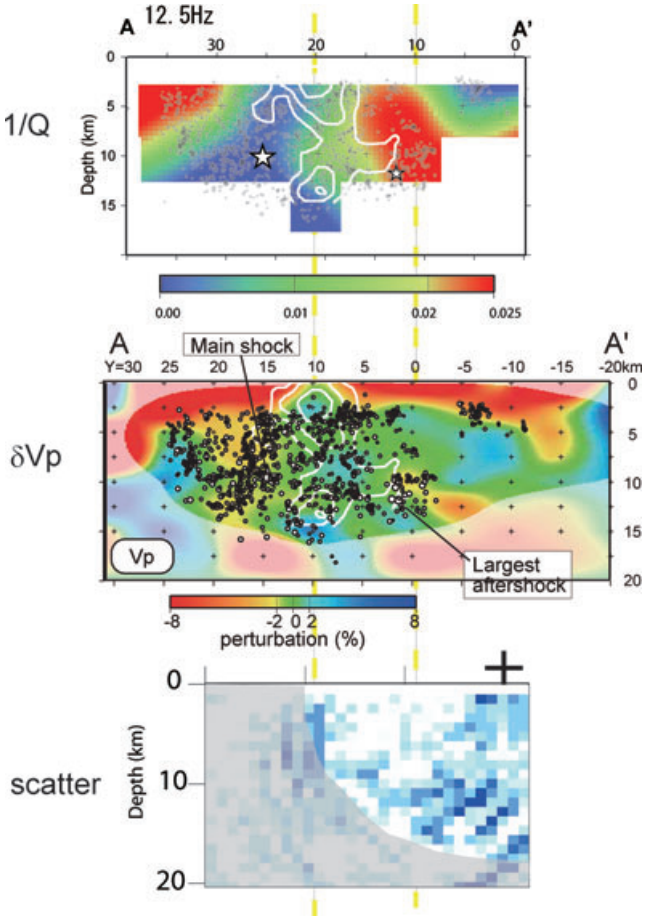

Figure 12. Comparison of the $1/Q$ distribution with velocity perturbation of P wave (dVp), scatterer, and seismic activity: (a) $1/Q$ distribution at 12.5 Hz and (b) dVp estimated by Hori *et al.* (2006). The white contour denotes the slip distribution proposed by Asano & Iwata (2006). (c) Scatterer distribution estimated by Matsumoto *et al.* (2006) based on the seismic array observation. The shaded area denotes the value with low reliability. The yellow dashed lines indicate $x = 10$ and 20 km.

study and the velocity structure is about several kilometre, the above factors could not be evaluated. Thus, we should remark the possibilities pointed out above for the interpretation for the estimated values.

The $1/Q$ value is estimated independently at every gridpoint. These values are frequency dependent and $1/Q$ decrease with increasing frequencies. In this study, we do not discuss the frequency dependence of the $1/Q$ values for each gridpoint in detail because the estimation error varies significantly for both the grids and the frequency bands. It is difficult to obtain a reliable result regarding the frequency dependence of the $1/Q$ value. Therefore, we only discuss the general property of the dependence. As mentioned above, the $1/Q$ value estimated here is a combination of the effects of intrinsic and scattering attenuations even though it is difficult to separate them from estimated $1/Q$ value. We describe interpretation on the basis of both causes of attenuation. The intrinsic attenuation is mainly due to the viscoelastic property of medium. The material attenuating seismic wave is often modelled by coupling elastic and viscous media. For instance, a standard linear solid is used to explain frequency dependent $1/Q$. This simple model can express $1/Q$ having a peak frequency and strong frequency dependence. The obtained $1/Q$ decrease does not so steep with frequency, which cannot be explained the simple model but requires combination of many model having various viscocity to simulate the dependence (Liu *et al.* 1976). The seismic-wave attenuation due to scattering is mainly caused by the fluctuations in both velocity and density heterogeneity. The physical property of the medium randomly fluctuates with its correlation distance larger than the seismic wavelength considered in this study, and the $1/Q$ value decreases with increasing frequency. In this case, the $1/Q$ value would have a peak at frequencies below the analysed frequency range. The $1/Q$ value will become maximum when the wavelength of the seismic wave becomes comparable to the correlation length of the medium. Consequently, the medium in the aftershock area has a correlation distance larger than a few kilometres (i.e. the wavelength of seismic wave analysed in this study) if we can assume that the scattering effect is the major factor in the attenuation mechanism.

In this study, we focus on the heterogeneity of the $1/Q$ structure of a P wave and discuss the relationship between the spatial distribution of the $1/Q$ value and other seismic structures. In Fig. 10, the low $1/Q$ region appears in a deeper part of northwestern half of the fault and extends to a shallower region in the middle part of the fault. The initiation point of the Fukuoka earthquake was located in the middle of this region. In the southeastern part [$(x, z) = (10, 10$ km)], the $1/Q$ value becomes high at frequencies higher than 7.5 Hz. High $1/Q$ in the southeastern edge of the fault segment of the earthquake is noticeable. The P-wave velocity anomaly reported by Hori *et al.* (2006) is shown in Fig. 12(b). We should pay attention the difference in the spatial resolutions of the $1/Q$ to the velocity structure. The velocity perturbations were estimated at every 2.5 km in depth and 10 km in horizontal, which is better resolution than the $1/Q$ estimation. Comparing our result with the velocity distribution, however, we can find some spatial relationship between them. The low $1/Q$ region around the hypocentre of the Fukuoka earthquake corresponds to moderately low velocity region. High aftershock activity is also seen in the low $1/Q$ region where the velocity anomaly is not remarkable. The velocity becomes low around the northwestern part [$(x, z) = (35, 5$ km)] and the southeastern part (10, 10 km).

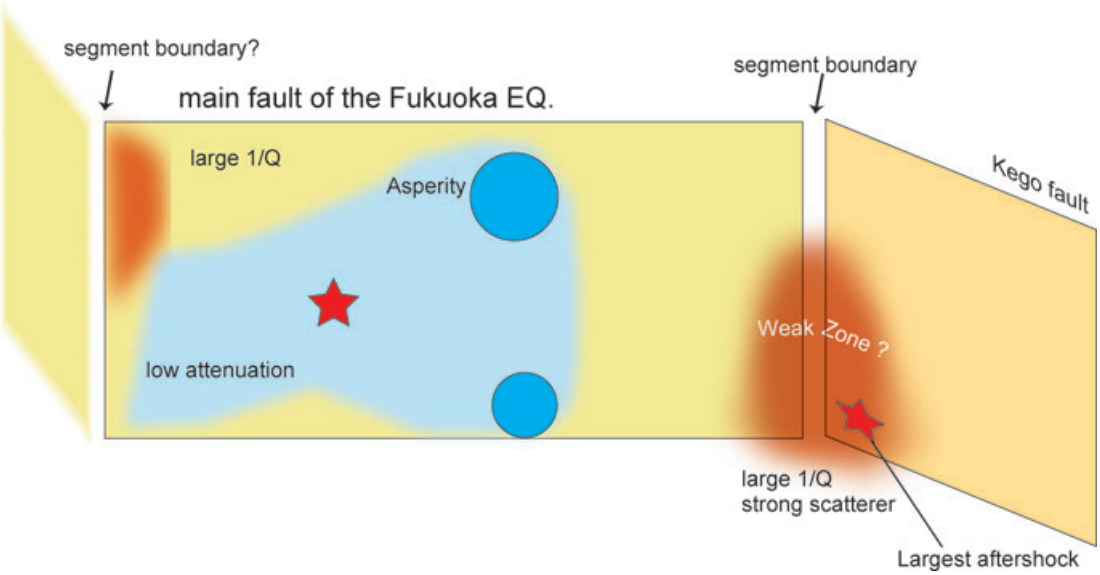

Figure 13. Model of the structure of the faults off Fukuoka. High attenuation takes place just below the asperity of the earthquake and at the segment boundary of the main fault and Kego fault. Large slips and high aftershock activities are observed in a region with low attenuation.

Table 1. Relationship between medium property and seismic activity.

	Main shock		Aftershock	
Seismic activity	Initial point	Asperity	High activity	Low activity
Velocity	Mod	High	Mod	Low
$1/Q$	Low	Low	Low	High

The slip distribution of the main shock reported by Asano & Iwata (2006) is plotted in Fig. 12(b). The contour line shows iso-slip lines at distances of 0.8, 1.6 and 2.4 m from the outer part. A large slip area is found at (20, 15 km) in relatively low $1/Q$ and high velocity regions. Because the $1/Q$ value in the shallower part where the largest slip occurred (called 'asperity') has not been estimated, we cannot discuss the relationship between the low $1/Q$ and the high-velocity regions in more detail. However, another asperity in the deeper part appears in the low $1/Q$ area. The medium having high strength generates large coseismic slips and therefore can exhibit low attenuation. We can also interpret the aftershocks that occurred in a 'weak heterogeneous zone' on the basis of the moderate velocity anomaly. Earthquakes with large slips occur in mediums with high velocity and low heterogeneity, with long wavelengths. In contrast, earthquakes with small slips, that is, small magnitude, can occur in the low heterogeneous zone with short wavelengths, although they do not always have high velocity. In Fig. 12(c), the scatterer distribution reported by Matsumoto *et al.* (2006) is shown. Based on seismic array observations, they identified relatively strong scatterers using array processing that determines coherent waves in the coda part, yielding the distribution. Strong scatterers exist around the southeastern part corresponding to the high $1/Q$ region. The scatterer distribution is estimated for the *S* waves of natural earthquakes. Although the mechanism of *S*-wave scattering is not always the same as that of *P*-wave attenuation, this scattering would strongly contribute to the attenuation mechanism of *P* waves. This fact provides the evidence for the existence of an inhomogeneous structure at the southeastern edge of the fault.

We summarize the relationship between the features of $1/Q$ and velocity and seismic activities in Table 1. Fig. 13 shows a simple model for the inhomogeneous structure of the Fukuoka earthquake. The large slip and high aftershock activity of the main shock fault are mostly found in and around the low $1/Q$ region. This suggests that low $1/Q$ would correlate to the relatively high strength on the fault. However, the largest aftershock and the following aftershocks have a different strike angle identical to the Kego fault, as described by Uehira *et al.* (2006). This finding implies that the rupture of the main shock stopped in the southeastern part of the fault and then the largest aftershock occurred on a different fault. In other words, a segment boundary exists between the main shock fault and the Kego fault. The present result reveals that the high $1/Q$ region extends from the segment boundary to the Kego fault. At this segment boundary, the $1/Q$ value is high, relative scattering strength is high, and *P*-wave velocity is low. These findings suggest that the segment boundary would have low strength due to the fault bending at this region. This could be a reason why the rupture stopped at the segment boundary.

CONCLUSIONS

We have developed a method for estimating with high resolution the seismic attenuation ($1/Q$) structure in hypocentral regions. We employed two seismograms recorded at a station and calculate the ratio between two power spectra of direct waves normalized by those in the coda for both the events in order to minimize the possible influences of sources, sites, instruments, and attenuation from the station to the hypocentral area. The event pairs were carefully selected to retain ray-path similarity of the direct waves between the pair of events. The $1/Q$ value can be estimated from the variation of the ratios of event pairs calculated at many stations for various traveltime differences between the even pairs. This method involves DD estimation from the logarithmic power spectra for estimating the $1/Q$ structure, employing a concept similar to the recently developed 'DD tomography' for velocity structures.

This method is applied to the data of the Fukuoka earthquake obtained from a seismic network. The frequency-dependent $1/Q$ structure in the aftershock area of the earthquake has revealed several spatial characteristics as indicated below.

1. A high $1/Q$ region is found in the segment boundary between the main shock fault and the Kego fault. This segment boundary has high $1/Q$ and high scattering strength, which could suppress the rupture of the main shock.
2. In the case of most of the aftershocks, the initiation points of the main shock and major slips with the main shock are found in the low $1/Q$ region.

The estimated $1/Q$ structure is in the wavenumber range between 1 km and a few hundreds of metres, yielding the inhomogeneous structure in this range. The present results suggest a possible relationship between $1/Q$ and the occurrence of earthquakes. For further confirmation of this relationship, it is necessary to apply the present method to a region where seismic and aseismic slips have occurred at the plate boundaries.

ACKNOWLEDGMENTS

We would like to express our gratitude to Prof Trampert, Prof Sato and two anonymous reviewers. Their comments and critical discussions helped us in improving our manuscript significantly. We are grateful for the cooperation of the members of Hokkaido University, Tohoku University, University of Tokyo, Kyoto University, Kagoshima University and Kyushu University during the temporary observations. The seismic data were obtained from JMA, Hi-net (NIED) and government of Fukuoka city.

REFERENCES

Aki, K., 1980. Attenuation of shear-waves in the lithosphere for frequencies from 0.05 to 25 Hz, *Phys. Earth planet. Inter.,* **21,** 50–60.

Aki, K. & Chouet, B., 1975. Origin of coda wave: source, attenuation and scattering effects, *J. geophys. Res.,* **80,** 3322–3342.

Asano, K. & Iwata, T., 2006. Source process and near-source ground motions of the 2005 West Off Fukuoka Prefecture Earthquake, *Earth Planets Space,* **58**(1), 93–98.

Blakeslee, S., Malin, P. & Alvarez, M., 1989. Fault-zone attenuation of high-frequency seismic wave, *Geophys. Res. Lett.,* **16**(11), 1321–1324.

Chun, K.-Y., West, G.F., Kokoski, R.J. & Samson, C., 1987. A novel technique for measuring Lg attenuation results from Eastern Canada between 1 to 10 Hz, *Bull. seism. Soc. Am.,* **77**(2), 398–419.

Chun, K.-Y., Henderson, G.A. & Liu, J., 2004. Temporal changes in P wave attenuation in the Loma Prieta rupture zone, *J. geophys. Res.,* **109,** B02317, doi:10.1029/2003JB002498.

De Lorenzo, S., Zollo, A. & Mongelli, F., 2001. Source parameters and three-dimensional attenuation structure from the inversion of microearthquake pulse width data: Qp imaging and inferences on the thermal state of the Campi Fligrei caldera (southern Italy), *J. geophys. Res.,* **106**(B8), 16265–16286.

Fehler, M., Hoshiba, M., Sato, H. & Obara, K., 1992. Separation of scattering and intrinsic attenuation for the Kanto-Tokai region, Japan, using measurements of S-wave energy versus hypocentral distance, *Geophys. J. Int.,* **108,** 787–800.

Hori, M. *et al*., 2006. 3D seismic velocity structure as determined by double-difference tomography in and around the focal area of the 2005 west off Fukuoka prefecture earthquake, *Earth Planets Space,* **58,** 1621–1626.

Hoshiba, M., 1993. Separation of scattering attenuation and intrinsic absorption in Japan using the multiple lapse time window analysis of full seismogram envelope, *J. geophys. Res.,* **98,** 15809–15824.

Kuwahara, Y., Ito, H., Kawakatsu, H., Ohminato, T. & Kiguchi, T., 1997. Crustal heterogeneity as inferred from seismic coda wave decomposition by small-aperture array observation, *Phys. Earth planet. Inter.,* **104,** 247–256.

Liu, H.P., Anderson, D.L. & Kanamori, H., 1976. Velocity dispersion due to anelasticity: implications for seismology and mantle composition, *Geophys. J. R. astr. Soc.,* **47,** 41–59.

Matsumoto, S., Watanabe, A., Matsushima, T., Miyamachi, H. & Hirano, S., 2006. Imaging S-wave scatterer distribution in south-east part of the focal area of the 2005 West off Fukuoka Prefecture Earthquake (M_{JMA}7.0) by dense seismic array, *Earth Planets Space,* **58,** 1627–1632.

Mayeda, K. & Walter, W.R., 1996. Moment, energy, stress drop, and source spectra of western United States earthquakes from regional coda envelopes, *J. geophys. Res.,* **101**(B5), 11195–11208.

Menke, W., 1989. *Geophysical Data Analysis: Discrete Inverse Theory*, revised edn, Academic Press, San Diego.

Nakao, S., Takahashi, H., Matsushima, T., Kohno, Y. & Ichiyanagi, M., 2006. Postseismic deformation following the 2005 West Off Fukuoka Prefecture Earthquake (M7.0) derived by GPS observation, *Earth Planets Space,* **58,** 1617–1620.

Peng, Z., Ben-Zion, Y., Michael, A.J. & Zhu, L., 2003. Quantitative analysis of seismic fault zone waves in the rupture zone of the 1992 Landers, California, earthquake: evidence for a shallow trapping structure, *Geophys. J. Int.,* **155,** 1021–1041.

Rautian, T.G., Khalturin, V.I., Martynov, V.G. & Molnar, P., 1978. Preliminary analysis of the spectral content of P and S waves from local earthquakes in the Gram Tadjikistan region*, Bull. seism. Soc. Am.,* **68**(4), 949–971.

Sato, H., 1977. Energy propagation including scattering effect: single isotropic scattering approximation, *J. Phys. Earth,* **25,** 17–41.

Sato, H. & Fehler, M., 1998. *Seismic Wave Propagation and Scattering in the Heterogeneous Earth*, AIP Press/Springer Verlag, New York, pp. 1–308.

Sato, T. & Hirasawa, T., 1973. Body wave spectra from propagating shear cracks, *J. Phys. Earth,* **21,** 415–431.

Schurr, B., Asch, G., Rietbrock, A., Trumbull, R. & Haberland, C., 2003. Complex patterns of fluid and melt transport in the central Andean subduction zone revealed by attenuation tomography, *Earth planet. Sci. Lett.,* **215,** 105–119.

Shimizu, H. *et al*., 2006. Aftershock seismicity and fault structure of the 2005 West Off Fukuoka Prefecture Earthquake (MJMA7.0) derived from urgent joint observations, *Earth Planets Space,* **58,** 1599–1604.

Smith, W.H.F. & Wessel, P., 1990. Gridding with continuous curvature splines in tension, *Geophysics,* **55,** 293–305.

Tsumura, N., Matsumoto, S., Horiuchi, S. & Hasegawa, A., 2000. Three-dimensional attenuation structure beneath the northeastern Japan arc estimated from spectra of small earthquakes, *Techtonophysics,* **319**(3), 241–260.

Uehira, K. *et al*., 2006. Precise aftershock distribution of the 2005 West Off Fukuoka Prefecture Earthquake (Mj = 7.0) by using a dense onshore and offshore seismic network, *Earth Planets Space,* **58,** 1605–1610.

Wagner, G.S., 1998. Local wave propagation near the San Jacinto fault zone, southern California: observations from a three-component seismic array, *J. geophys. Res.,* **103,** 7231–7246.

Waldhauser, F. & Ellsworth, W.L., 2000. A double-difference earthquake location algorithm: method and application to the northern Hayward Fault, *California, Bull. seism. Soc. Am.,* **90,** 1353–1368.

Walter, W.R., Mayeda, K., Malagnini, L. & Scognamiglio, L., 2007. Regional body-wave attenuation using a coda source normalization method: application to MEDNET records of earthquakes in Italy, *Geophys. Res. Lett.,* **34,** L10308, doi:10.1029/2007GL029990.

Yoshimoto, K., Sato, H. & Ohtake, M., 1993. Frequency-dependent attenuation of P and S waves in the Kanto area, Japan, based on the coda-normalization method, *Geophys. J. Int.,* **114,** 165–174.

Zhang, H. & Thurber, C., 2003. Double-difference tomography: the method and its application to the Hayward Fault, California, *Bull. seism. Soc. Am.,* **93,** 1875–1889.